

Synthetically tuneable biomimetic artificial photosynthetic reaction centres that closely resemble the natural system in purple bacteria

Sai-Ho Lee,^a Iain M. Blake,^a Allan G. Larsen,^a James A. McDonald,^a Kei Ohkubo,^b Shunichi Fukuzumi,^{*c,d} Jeffrey R. Reimers^{*a,e,f} and Maxwell J. Crossley^{*a}

^a*School of Chemistry F11, The University of Sydney, 2006, NSW, Australia. E-mail: maxwell.crossley@sydney.edu.au*

^b*Department of Material and Life Science, Graduate School of Engineering, Osaka University, Suita, Osaka 565-0871, Japan. E-mail: fukuzumi@chem.eng.osaka-u.ac.jp*

^c*Department of Chemistry and Nano Science, Ewha Womans University, Seoul 120-750, Korea*

^d*Faculty of Science and Engineering, Meijo University, Nagoya, Aichi 468-0073, Japan.*

^e*International Centre for Quantum and Molecular Structure, Shanghai University, 200444, Shanghai, China. E-mail: reimers@shu.edu.cn*

^f*School of Mathematical and Physical Sciences, The University of Technology Sydney, 2007, NSW, Australia. E-mail: jeffrey.reimers@uts.edu.au*

Electronic Supplementary Information

S1. Synthesis

S2. Steady-state absorption and emission spectroscopy

S3. Electrochemistry

S4. Fitting of Data Measured by Femtosecond Laser Flash Photolysis

S5. Spectroelectrochemistry of (2HP)₂

S6. Vibrational Parameters Deduced for the Molecular Fragments from B3LYP Vibrational Frequency Analysis

S7. References

S1. Synthesis

Synthesis of zinc(II) 12/13-nitro-{(formylphenyl)imidazo}porphyrins 2. A mixture of the zinc(II) 12-nitroporphyrin-2,3-dione **1**¹ (296 mg, 0.246 mmol), terephthalaldehyde (198 mg, 1.48 mmol) and ammonium acetate (370 mg, 4.80 mmol) in ethanol-free CHCl₃ (40 ml) was heated at reflux with stirring in the dark for 1 hour. The reaction mixture was diluted with CH₂Cl₂ (100 ml) and washed with water (2 × 100 ml), dried over anhydrous Na₂SO₄, filtered and the solvent removed. The residue was purified by column chromatography on silica, (CH₂Cl₂). The major green band collected and the solvent removed. The residue was crystallised from a CH₂Cl₂/CH₃OH mixture to give zinc(II) 12- and 13-nitro-{(formylphenyl)imidazo}porphyrins **2** (291 mg, 90 %) as a dark green powder. UV-Vis λ_{\max} (CHCl₃)/nm 345 (log ϵ 4.29), 388 (4.44), 443 (5.30), 523 (3.62), 558 (4.29) and 596 (3.77); IR ν_{\max} (CHCl₃)/cm⁻¹ 3429w (imidazole NH), 2964s, 2905w, 2870w, 1701s (CHO), 1608s, 1591m, 1525w, 1477m, 1394w, 1364m, 1339w, 1248m, 1199m, 1169w, 1111w and 1009w; ¹H NMR δ_{H} (300 MHz; CDCl₃) 1.52–1.54 (72H, m, *t*-C₄H₉), 7.76–7.77 (1H, m, aryl H_p), 7.81–7.83 (1H, m, aryl H_p), 7.89–7.91 (3H, m, 2 × phenyl H, 1 × aryl H_p), 7.98 (2H, AA' of AA'BB' system, phenyl H), 8.03–8.05 (4H, m, 1 × aryl H_p, 3 × aryl H_o), 8.09–8.10 (5H, m, aryl H_o), 8.60 (1H, bs, imidazole NH), 8.94–9.09 (4H, m, β -pyrrolic H), 9.18–9.19 (1H, m, β -pyrrolic H), 10.05 (1H, s, CHO); MALDI-TOF m/z 1286 ([M – CHO]⁺, 100 %); HR-MS (ESI) C₈₄H₉₅N₇O₃Zn [M + H]⁺ 1316.68713 calculated, 1316.68266 obtained.

Synthesis of 12/13-nitro-{(fullerene-N-methylpyrrolidinyl-phenyl)imidazo}porphyrins 3. A solution of zinc(II) 12/13-nitro-{(formylphenyl)imidazo}porphyrins **2** (544 mg, 0.013 mmol) in CH₂Cl₂ (100 ml) was treated with hydrochloric acid (7M, 50 ml) and stirred vigorously for 15 min. CH₂Cl₂ (100 ml) was added and the organic layer washed with water (2 × 100 ml), a sodium carbonate solution (10 %, 100 ml) and water (100 ml), dried over anhydrous Na₂SO₄, filtered and the solvent removed. The residue was purified using column chromatography over silica (CH₂Cl₂/hexane; 3:1) to yield free-base 12/13-nitro-{(formylphenyl)imidazo}porphyrin (460 mg, 89 %) as a brown powder. A mixture of free base 12 and 13-nitro-{(formylphenyl)imidazo}porphyrin (216 mg, 0.17 mmol), C₆₀ (125 mg, 0.17 mmol) and *N*-methylglycine (52 mg, 0.58 mmol) in dry toluene was heated at reflux for 20 hours. The solvent was removed and the residue was purified by column chromatography on silica, (CH₂Cl₂/hexane; 3:1). The major dark brown band collected and the solvent removed. The residue was **recrystallized** from a CH₂Cl₂/CH₃OH mixture to give 12/13-nitro-{(fullerene-*N*-methylpyrrolidinylphenyl)imidazo}porphyrin] **3** (254 mg, 75 %) as a dark brown powder. UV-Vis λ_{\max} (CHCl₃)/nm 435 (log ϵ 5.30), 532 (4.27), 547 (3.84) and 660 (3.86); IR ν_{\max} (CHCl₃)/cm⁻¹ 3431w (imidazole NH), 3337w (inner NH), 2964s, 2905w, 2868w, 1591m, 1558w, 1477m, 1427m, 1394w, 1292m, 1246m, 1171m, 1097w, 1032w, 926w, 883w, and 854w; ¹H NMR δ_{H} (300 MHz; CDCl₃) -2.68–2.57 (2H, m, inner NH), 1.45–1.50 (36H, m, *t*-C₄H₉), 1.52–1.53 (36H, m, *t*-C₄H₉), 2.82 (3H, s, NCH₃), 4.19 (1H, d, *J* 9.4 Hz, CH₂), 4.87–4.90 (2H, m, CH + CH₂), 7.69–7.84 (5H, m, phenyl H, aryl H_p), 8.03–8.09 (11H, m, aryl H_p, H_o), 8.21–8.27 (1H, m, imidazole NH), 8.88–9.12 (5H, m, β -pyrrolic H); MALDI-TOF m/z 1279 ([M – fullerene]⁺, 30 %), 1234 ([M – fullerene – NO₂]⁺, 100 %); HR-MS (ESI) C₁₄₆H₁₀₂N₈O₂ [M + 2H]²⁺ 1000.91519 calculated, 1000.91295 obtained.

Synthesis of {6'-(3,4-diaminobenzene)quinoxalino}-{(fullerene-*N*-methylpyrrolidinylphenyl)imidazo}porphyrin 5. A mixture of 12/13-nitro-{(fullerene-*N*-methylpyrrolidinylphenyl)imidazo}porphyrin **3** (98 mg, 0.05 mmol) and tin (II) chloride dihydrate (241 mg, 1.05 mmol) in hydrochloric etherate (50 ml) was stirred in the dark for 5 min at RT. The mixture was poured onto water (50 ml) and CH₂Cl₂ (100 ml) added. The organic layer was repeatedly washed with water (5 × 100 ml), dried over anhydrous Na₂SO₄, filtered and the solvent removed. The residue was dissolved in CH₂Cl₂ (250 ml), photo-oxidized for 2 hours and the solvent removed. The residue was purified by column chromatography on silica, (CH₂Cl₂/hexane; 3:1). The major olive band collected and the solvent removed to yield 12,13-dioxo-{(fullerene-*N*-methylpyrrolidinylphenyl)imidazo}porphyrin **4** (52 mg, 54 %). 12,13-Dioxo-{(fullerene-*N*-methylpyrrolidinyl-phenyl)imidazo}porphyrin **4** was dissolved in CH₂Cl₂ (50 ml) and added drop wise to a stirred solution (suspension) of 3,3'-diaminobenzidine (107 mg, 0.50 mmol) in CH₂Cl₂ (250 ml) over 1 hour. The mixture was stirred at RT in the dark for 48 hours. The solvent was removed and the brown residue purified by column chromatography over silica, (CH₂Cl₂ /hexane; 3:2 then CH₂Cl₂/CH₃OH; 10:1). The major polar brown band collected and the solvent removed. The residue was crystallised from a CH₂Cl₂/CH₃OH mixture to give {6'-(3,4-diaminobenzene)quinoxalino}-{(fullerene-*N*-methyl-pyrrolidinylphenyl)imidazo}porphyrin **5** (46 mg, 80 %) as a brown powder. UV-Vis λ_{\max} (CHCl₃)/nm 439 (log ϵ 5.19), 527 (4.36), 561 (3.89), 602 (4.06), and 655 (3.76); IR ν_{\max} (CHCl₃)/cm⁻¹ 3439w (imidazole NH), 3361w (inner NH), 2962s, 2926s, 2856m, 1733w, 1591m, 1492w, 1460m, 1427w, 1393w, 1364m, 1294w, 1248m, 1148w, 1122m, 1034w, 918w, 899w, and 879w; ¹H NMR δ_{H} (300 MHz; CDCl₃) -2.85 (1H, bs, inner NH), -2.70 (1H, bs, inner NH), 1.49–1.52 (72H, m, *t*-C₄H₉), 2.77 (3H, s, NCH₃), 3.50 (4H, v.bs, NH₂), 4.09 (1H, d, *J* 10 Hz, CH₂), 4.78–4.86 (2H, m, CH + CH₂), 6.71–6.90 (1H, m), 7.11–7.17 (2H, m), 7.73–7.88 (5H, m), 7.93–8.27 (15H, m), 8.96–9.11 (4H, m, β -pyrrolic H); MALDI-TOF *m/z* 1444 ([M – fullerene]⁺, 100 %); HR-MS (ESI) C₁₅₈H₁₁₁N₁₁ [M + H]⁺ 2163.91305 calculated, 2163.91044 obtained.

Synthesis of (12/13-nitro-quinoxalino)-{(fullerene-imidazo)quinoxalino}bisporphyrin 7. A mixture of {6'-(3,4-diaminobenzene)quinoxalino}-{(fullerene-*N*-methylpyrrolidinylphenyl)imidazo}porphyrin **5** (46 mg, 0.021 mmol) and 12-nitroporphyrin-dione **6** (26 mg, 0.023 mmol) in CH₂Cl₂ (20 ml) was stirred at RT, in the dark for 5 days. The solvent was removed and the residue purified by column chromatography over silica, (CH₂Cl₂/hexane; 2:1). The major brown band collected and the solvent removed. The residue was crystallised from a CH₂Cl₂/CH₃OH mixture to give (12/13-nitro-quinoxalino)-{(fullerene-imidazo)quinoxalino}bisporphyrin **7** (39 mg, 56 %) as a brown powder. UV-Vis λ_{\max} (CHCl₃)/nm 451 (log ϵ 5.46), 532 (4.77), 604 (4.39) and 655 (3.94); IR ν_{\max} (CHCl₃)/cm⁻¹ 3433w (imidazole NH), 3362w (inner NH), 2964s, 2903m, 2868m, 1593m, 1473w, 1425m, 1394w, 1363m, 1348w, 1294m, 1248m, 1148m, 1124m, 920w, 901w, 881w, 854w, and 802w; ¹H NMR δ_{H} (300 MHz; CDCl₃) -2.82 (1 H, bs, inner NH), -2.66 (1 H, bs, inner NH), -2.26 (2 H, bs, inner NH), 1.45–1.58 (144 H, m, *t*-C₄H₉), 2.78–2.79 (3 H, m, NCH₃), 4.05–4.14 (1 H, m, CH₂), 4.83–4.89 (2 H, m, CH + CH₂), 7.73–7.85 (6 H, m), 7.98–8.17 (29 H, m), 8.95–9.16 (9 H, m, β -pyrrolic H); MALDI-TOF *m/z* 2545.5 ([M – fullerene]⁺, 100 %), 2500 ([M – fullerene – NO₂]⁺, 90 %); HR-MS (ESI) C₂₃₄H₁₉₈N₁₆O₂ [M + H]²⁺ 1633.804698 calculated, 1633.802898 obtained.

Synthesis of (Tröger's base-quinoxalino)-{(fullerene-imidazo)quinoxalino}trisporphyrin (2HP)₂Q-Q2HP-C₆₀. A mixture of (12/13-nitro-quinoxalino)-{(fullerene-imidazo)quinoxalino}bisporphyrin **7** (107 mg, 0.033 mmol), tin (II) chloride dihydrate (79 mg, 0.33 mmol) and hydrochloric acid (12 ml) in CH₂Cl₂ (15 ml) was stirred in the dark for 5 min at RT. The mixture was poured onto water (50 ml) and CH₂Cl₂ (80 ml) added. The organic layer was repeatedly washed with water (5 × 100 ml), dried over anhydrous Na₂SO₄, filtered and the solvent removed to give (12/13-amino-quinoxalino)-{(fullerene-imidazo)quinoxalino}bisporphyrin **8**. Without further purification, **8** was dissolved in dry THF (10 ml), 2-amino-5,10,15,20-tetrakis-(3,5-di-tert-butylphenyl)porphyrin **9** (75 mg, 0.069 mmol) added and the solution degassed with argon. Hydrochloric acid (10 M, 0.7 ml) in ethanol (1.5 ml) and formaldehyde (37 % aqueous solution, 0.21 ml) was added and the mixture stirred in the dark under nitrogen for 4 days at 70 °C. The mixture was extracted into CHCl₃ (2 x 10 ml) and the organic phase washed with water (40 ml), dried over anhydrous Na₂SO₄, filtered and the solvent removed. The residue was purified by size exclusion chromatography (sephadex SX-1), toluene. The second band collected and the solvent removed. The residue was further purified by crystallization from a CH₂Cl₂/CH₃OH mixture to yield (Tröger's base-quinoxalino)-{(fullerene-imidazo)quinoxalino}trisporphyrin **(2HP)₂Q-Q2HP-C₆₀** (23 mg, 16 %) as a brown powder. UV-Vis λ_{\max} (CHCl₃)/nm 424 (log ϵ 5.55), 532 (4.88), 604 (4.33), 656 (4.02) and 674sh (3.94); IR ν_{\max} (CHCl₃)/cm⁻¹ 3439w (imidazole NH), 3356w (inner NH), 2964s, 2868m, 1593m, 1477w, 1427m, 1393w, 1364m, 1296m, 1247m, 1148m, 1107m, 920w, 901w and 883w; ¹H NMR δ_{H} (300 MHz; CDCl₃) -3.37–-3.07 (2 H, vbs, inner NH), -3.01 (1 H, bs, inner NH), -2.83 (2H, bs, inner NH), -2.66, (2 H, bs, inner NH), 1.22–1.58 (216 H, m, *t*-C₄H₉), 2.83 (3 H, bs, NCH₃), 3.42–3.49 (2 H, m, Tröger's base methylene H), 3.90–3.99 (2 H, m, Tröger's base methylene H), 4.16–4.21 (1 H, m, CH₂), 4.30 (2H, bs, Tröger's base bridge CH₂), 4.88–4.93 (2 H, m, CH + CH₂), 6.87–6.93 (1 H, m), 6.99–7.03 (1 H, m), 7.17–7.34 (2 H, m), 7.36–7.40 (3 H, m), 7.57–8.20 (42 H, m), 8.26–8.30 (1H, m), 8.34–8.37 (1 H, m), 8.45–8.55 (1 H, m), 8.70–8.81 (2 H, m), 8.84–8.91 (2 H, m), 9.01–9.17 (3 H, m); MALDI-TOF *m/z* 3630.3 ([M – fullerene]⁺, 100 %); HR-MS (ESI) C₃₁₃H₂₉₅N₂₁ [M + 2H]²⁺ 2176.19882 calculated, 2176.19404 obtained.

Synthesis of (di-zinc(II) Tröger's base-quinoxalino)-{(fullerene-imidazo)quinoxalino}trisporphyrin (ZnP)₂Q-Q2HP-C₆₀. (Tröger's base-quinoxalino)-{(fullerene-imidazo)quinoxalino}trisporphyrin **(2HP)₂Q-Q2HP-C₆₀** (10 mg, 0.0023 mmol) was dissolved in CH₂Cl₂ (5 mL) and zinc acetate dihydrate (0.5 mg, 0.0023 mmol) was added as a solution in CH₃OH (1 mL). The reaction was stirred at RT for 30 mins to yield the mono-metallated product. After this time, a second equivalent of zinc acetate dihydrate (0.5 mg, 0.0023 mmol) was added, again, as a solution in CH₃OH (1 mL). The reaction was stirred at RT for a further 3 h when complete insertion into the second macrocycle was observed. The reaction mixture was passed through a short silica plug and the product was purified further on a silica column (CH₂Cl₂/hexane 2:1). The product was crystallised from CHCl₃/CH₃OH mixture to give (di-zinc(II) Tröger's base-quinoxalino)-{(fullerene-imidazo)quinoxalino}-trisporphyrin **(ZnP)₂Q-Q2HP-C₆₀** (6 mg, 58%). UV-Vis λ_{\max} (PhCN)/nm 432 (log ϵ 5.54), 527 (4.88), 565 (4.73), 604 (4.76), 639 (4.41) and 655sh (4.37); ¹H NMR δ_{H} (400 MHz; CDCl₃) -2.82 (1 H, s, inner NH), -2.67 (1 H, s, inner NH), 1.19–1.58 (216 H, m, *t*-C₄H₉), 2.75–2.97 (3 H, m, NCH₃), 3.18 (1 H, s, Tröger's base methylene H), 3.43–3.56 (1 H, m, Tröger's base methylene H), 3.79–3.92 (1 H, m, CH₂), 4.11–4.32 (2 H, m, Tröger's base methylene H), 4.68 (2H, s, Tröger's base bridge CH₂), 4.94 (2 H,

bs, CH + CH₂), 6.45–6.57 (1 H, d), 7.00 (1 H, s), 7.18–7.55 (12 H, m), 7.56–7.67 (4 H, m), 7.69–7.92 (12 H, m), 7.93–8.24 (19 H, m), 8.25–8.33 (2 H, m), 8.44 (1H, bs), 8.56–8.62 (1 H, m), 8.71–8.77 (1 H, m), 8.80–8.90 (2 H, m), 8.90–8.99 (2 H, m), 9.03–9.22 (3 H, m); HR-MS (ESI) C₃₁₃H₂₉₁N₂₁Zn [M + 2H]²⁺ 2239.11071 calculated, 2239.15427 obtained, [M + 2H - CH₃]²⁺ 2224.13852 obtained.

S2. Steady-State absorption and emission spectra

Figures S1 and S2 compare absorption and emission spectra for **2HP**, **2HPQ**, **Q2HP-Ph** and **Q2HP-C₆₀**. The absorption spectra of **2HP** and **2HPQ** shown in Fig. S1a are consistent with those reported previously.²⁻⁴ The spectra consist of a strong Soret (B) band and four Q-band components, interpreted as comprising two alternatively polarized origin bands Q_x (lower frequency) and Q_y (higher frequency), each with a vibrational sideband at 1200 to 1500 cm⁻¹ higher frequency. Fusing the quinoxaline onto the porphyrin macrocycle splits the Soret (B) band. This effect for related molecules,⁵ with fused tetraazaanthracene instead of quinoxaline, has been interpreted as arising from the appearance of new porphyrin to quinoxaline charge-transfer bands near the Soret band, as well as splitting of the Soret B_x and B_y components. Both the Soret and in particular the Q_y bands show significant average red-shifts of 550 cm⁻¹ and 450 cm⁻¹, respectively, with also a small shift of ca. 100 cm⁻¹ for the lowest-energy band Q_x. All these spectral changes indicate the extension of π-conjugation. Quinoxaline fusion is also seen to invert the relative intensity of the origin and sidebands, indicating that in **2HPQ**, at least, the sideband intensity arises from vibronic rather than Franck-Condon means as Franck-Condon allowed sidebands are always much weaker than their origins in porphyrinic compounds.

The Q_x emission spectra shown in Fig. S1b illustrate the same inversion of the relative intensities of the origin and sidebands for **2HP** and **2HPQ** as seen in the absorption spectra, indicating that gross absorption/emission symmetry features are qualitatively maintained in these molecules. However, comparison of the absorption and emission spectra for each molecule individually reveals that the sidebands appear at only about a quarter of the relative intensity of the origin bands in emission compared to absorption. This apparent anomaly arises as the raw intensities need to be scaled for the frequency-dependence of the Einstein coefficients for

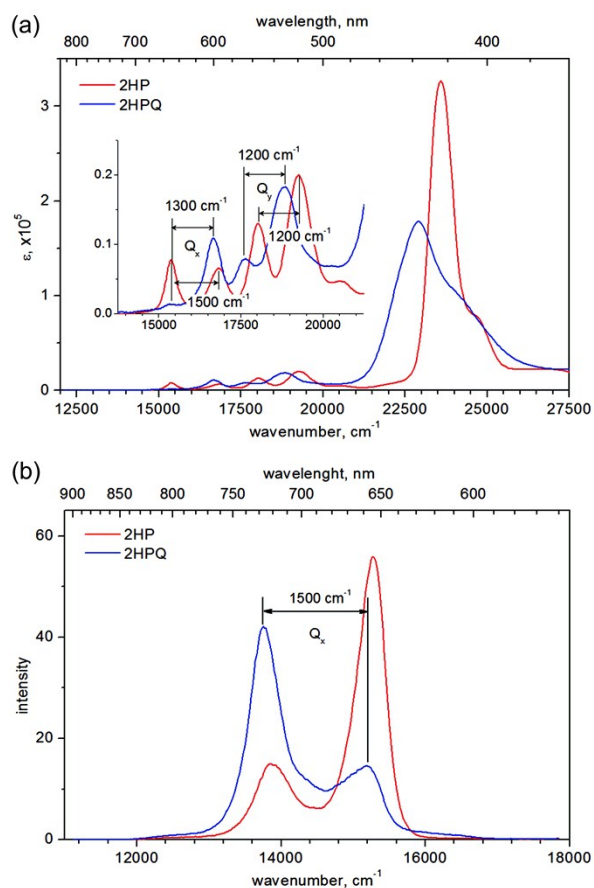


Fig. S1. (a) UV-visible absorption spectra indicating the molar extinction coefficients ϵ (in M⁻¹cm⁻¹), and (b) emission spectra following excitation at 550 nm of **2HP** and **2HPQ** in PhCN.

absorption and spontaneous emission, and the emission intensity normalized for plotting versus frequency, generating a scaling of $[(\Delta E - h\nu)/\Delta E]^6 = (14000/15500)^6 = 0.54$ where ΔE is the electronic transition origin energy and $h\nu$ the energy of the vibrational sideband. The power of 6 comes from the combination of the $\propto \nu^3$ scaling of spontaneous emission in the Einstein A coefficient, the $\propto \nu$ scaling of absorption in the Einstein B coefficient, and the $\propto \nu^2$ scaling coming from the transformation from wavelength to frequency as the emission spectra were recorded with wavelength being scanned linearly in time;⁶ this has a profound effect on perceived absorption/emission asymmetry and forms the basis of say the Planck radiation law but nevertheless is often poorly understood. In addition, as the sidebands arise from a vibronic interaction between the Q_y and B_x states, asymmetry appears in the line intensity that, according to Herzberg-Teller perturbation theory,⁷⁻¹¹ attains a ratio of emission to

$$\text{absorption of } \left(\frac{E_{B_x} - E_{Q_y} - h\nu_{\text{vib}}}{E_{B_x} - E_{Q_y} + h\nu_{\text{vib}}} \right)^2 \sim 0.4$$

Hence the observed absorption and emission spectra show some unusual properties that provide detailed support to the proposed spectral assignment. Therefore, the observed photochemical processes are all interpreted based on this assignment.

Figure S2a shows the absorption spectra of **2HPQ**, **Q2HP-Ph** and **Q2HP-C₆₀**. Considerable shifts of 70 to 110 cm^{-1} of the **Q2HP-Ph** and **Q2HP-C₆₀** Q bands occur when the phenyl ring is linked to the porphyrin by the imidazole, suggesting extended π conjugation. Spectral changes between **Q2HP-C₆₀** and **Q2HP-Ph** indicate that some intramolecular interactions occur between the porphyrin and fullerene but the primary qualitative identity of each chromophore is clearly preserved. On the other hand, the emission spectrum of **Q2HP-C₆₀** (Fig. S2b) illustrates a dramatic quench of 2HPQ fluorescence (λ_{max} at 15200 cm^{-1} and 13700 cm^{-1}) after photoexcitation, with respect to the control compound **Q2HP-Ph**. This suggests the occurrence of a new electronic process amongst the excited-state of **Q2HP-C₆₀** which is subsequently identified as primary charge-separation to form $\text{Q2HP}^{+\cdot}\text{-C}_{60}^{\cdot-}$. By co-plotting the absorption and emission spectra (Fig. S2c), the lowest energy of ${}^1\text{Q2HP}(\text{S}_1)^*$ is estimated to be 15000 cm^{-1} , which is equivalent to 1.89 eV, while the Stokes shift is found to be 100 cm^{-1} (Table 1).

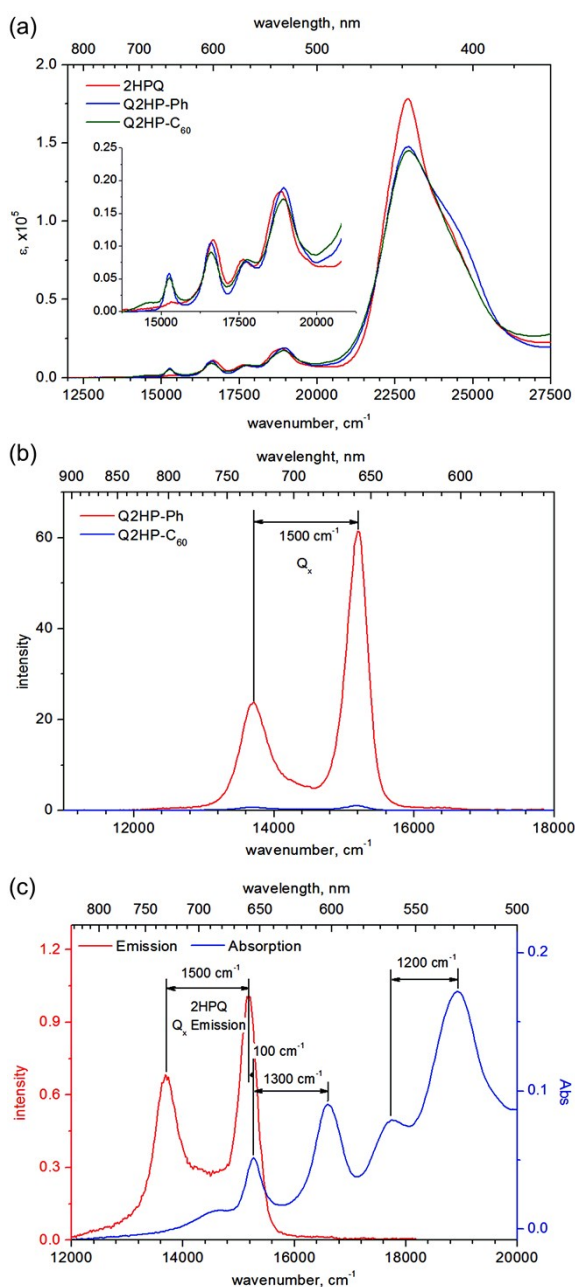


Fig. S2. (a) UV-visible absorption spectra, indicating the molar extinction coefficients ϵ (in $\text{M}^{-1}\text{cm}^{-1}$), and (b) emission spectra, following excitation at 550 nm, of **2HPQ**, **Q2HP-Ph** and **Q2HP-C₆₀** in PhCN. (c) Co-plot of emission and UV-visible absorption spectra of **Q2HP-C₆₀**.

Figure S3a shows the absorption spectrum of **ZnPQ-Q2HP-C₆₀**, and its model compounds **ZnPQ**, **Q2HP-Ph** and **Ph-C₆₀**. If there is no intramolecular interaction between the chromophores, the absorption spectrum would be the sum of the individual chromophoric spectra. The spectrum of **ZnPQ-Q2HP-C₆₀**, however, shows significant broadening of the Soret region compared to the sum of the spectra of **ZnPQ**, **Q2HP-Ph** and **Ph-C₆₀**. This broadening indicates intramolecular interactions through the biquinoxaliny (Qx-Qx) linkage and most likely arises as the Soret band interferes strongly with the porphyrin to quinoxaline transitions.⁵ Furthermore, a co-plot of the absorption and emission spectra of **ZnPQ-Q2HP-C₆₀** is shown in Fig. S3b. The emission of **ZnPQ-Q2HP-C₆₀**, strongly quenched due to the occurrence of electron transfer (not shown), displays only 2HPQ fluorescence with a Stokes shift of 100 cm⁻¹. As no **significant** ZnPQ fluorescence (expected at λ_{max} of 15700 cm⁻¹ and 14600 cm⁻¹)^{12, 13} is observed, this indicates that an intramolecular singlet-singlet energy-transfer occurs from the ZnPQ group (ca. 1.97 eV) to the energetically lower lying 2HPQ group (ca. 1.89 eV) upon photoexcitation.

This intramolecular singlet-singlet energy-transfer process is also identified in the subsequent time-resolved spectral study. A similar conclusion has been reached for some similar systems.¹⁴⁻¹⁸ Also shown in Fig. S3b, a weak absorption is observed near 14000 cm⁻¹ that arises from the fullerene moiety. The relative absorbances at 430 nm indicate that fullerene absorption accounts for ca. 5% of the light absorption at the excitation energy used in transient absorption studies.

The Tröger's base linked porphyrin dimer (**ZnP**)₂ shows significant spectral changes in absorption with respect to the monomeric porphyrin **ZnP** (Fig. S4a). These spectral changes include broadening and red-shifts of transition bands. Similar spectral changes are also observed for the free-base analogue (**2HP**)₂ (Fig. S4b). The shifts of the Q band transitions are determined to be 300 cm⁻¹ and 500 cm⁻¹ for (**ZnP**)₂ and (**2HP**)₂, respectively. These energy shifts could possibly be due to either the β -substitution attaching the Tröger's base linker and/or to exciton coupling between the chromophores.

The absorption and emission spectra of monomeric porphyrin **ZnP** and its Tröger's base porphyrin dimer (**ZnP**)₂ are shown in Fig. S4c. The spectra obtained are quite different from those presented earlier for the comparison of **2HPQ** with **2HP** and of **ZnPQ-Q2HP-C₆₀** with **ZnPQ** and **2HPQ**: large Stokes shifts are obtained and absorption/emission symmetry is reduced. The Stokes shifts are found to be 600 cm⁻¹ and 200 cm⁻¹ for (**ZnP**)₂ and **ZnP**, respectively, much larger than

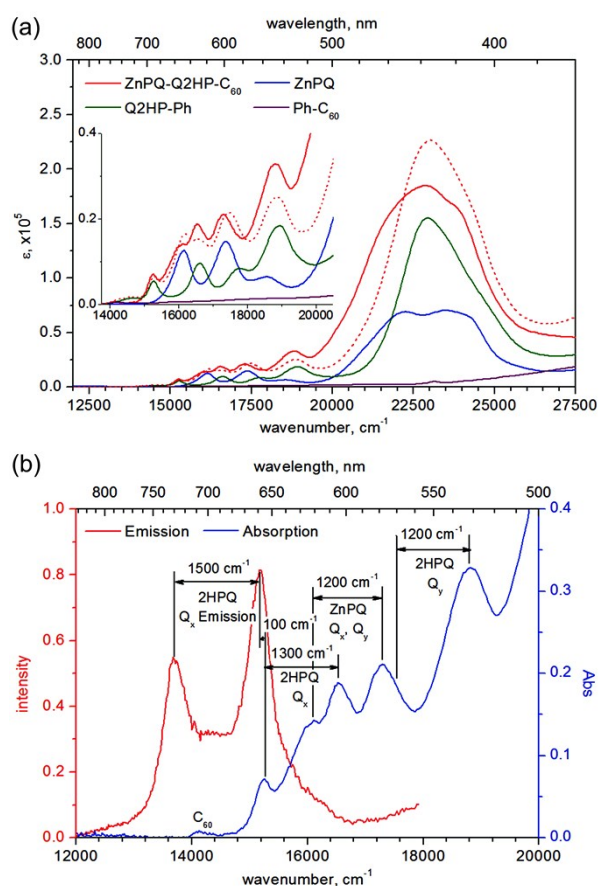


Fig. S3. (a) UV-visible absorption spectra indicating the molar extinction coefficients ϵ (in $M^{-1} \text{cm}^{-1}$) of **ZnPQ-Q2HP-C₆₀**, **ZnPQ**, **Q2HP-Ph** and **Ph-C₆₀** in PhCN; the short dotted line indicates the sum of **ZnPQ**, **Q2HP-Ph** and **Q2HP-C₆₀** spectra. (b) Co-plot of emission and UV-visible absorption spectra of **ZnPQ-Q2HP-C₆₀** in PhCN. The fluorescence experiment used excitation at 550 nm.

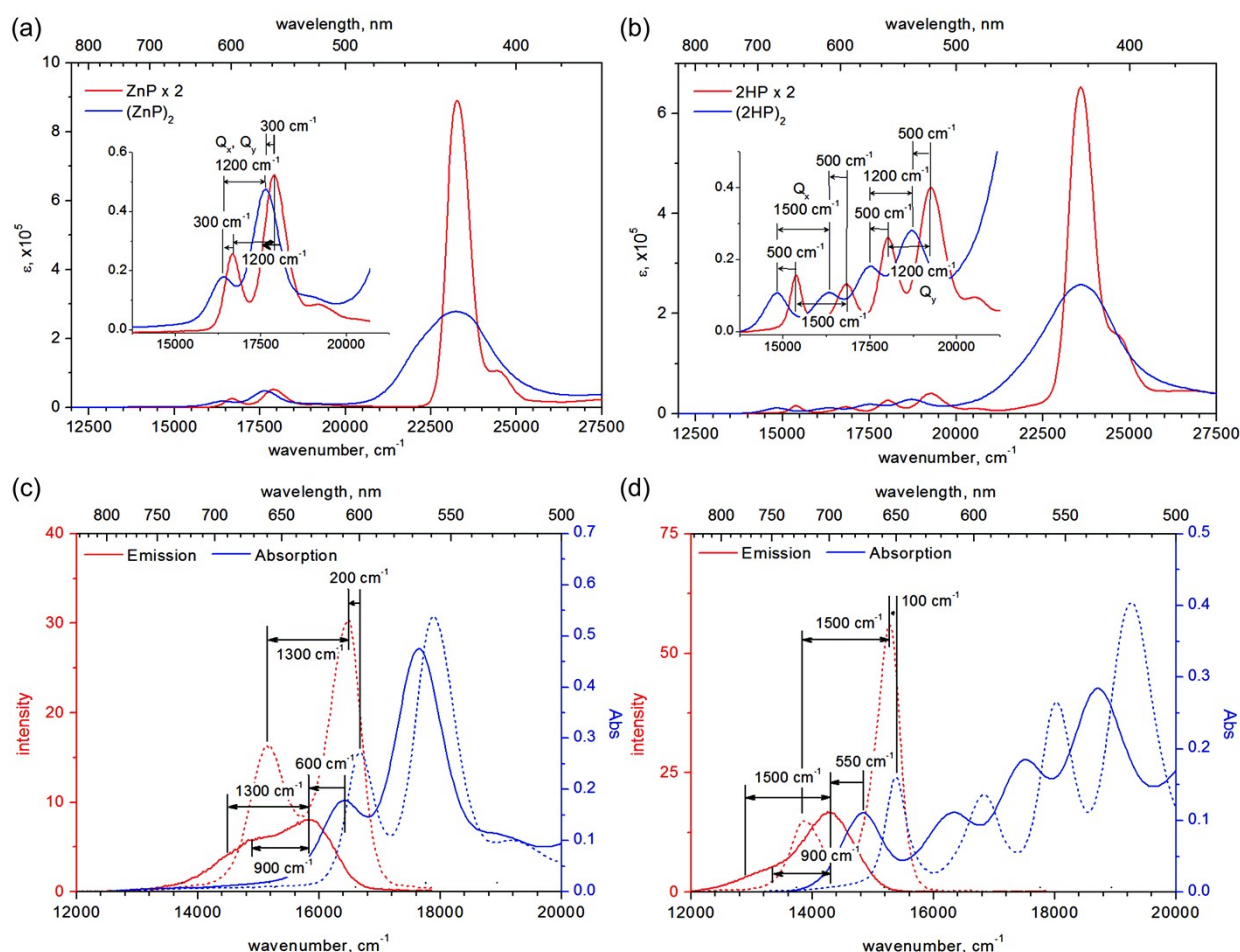


Fig. S4. UV-visible absorption spectra indicating the molar extinction coefficients ϵ (in $M^{-1} cm^{-1}$) of (a) **ZnP** and **(ZnP)₂**; and (b) **2HP**, and **(2HP)₂** in PhCN. Co-plot of emission and UV-visible absorption spectra of (c) **ZnP** (dotted line) and **(ZnP)₂** (solid line); and (d) **2HP** (dotted line) and **(2HP)₂** in PhCN. For the fluorescence experiment, a wavelength of 550 nm was used for excitation.

the previously determined value of 100 cm^{-1} for both **2HP** and **2HPQ**. Like **2HP** (Figure 3a), the emission sideband is much reduced in intensity compared to the absorption sideband. However, the emission of **(ZnP)₂** takes quite a different character. The main emission sideband at $\nu_{\text{vib}} = 1300\text{ cm}^{-1}$ appears strongly quenched, whilst new structure at $\nu_{\text{vib}} = 900\text{ cm}^{-1}$ is revealed. It is likely that this new band corresponds to a Tröger's base bending vibration that moves the porphyrins towards or away from each other. Taken together, these observations suggest that absorption of **(ZnP)₂** occurs at a configuration at which the excitation is localized on a single chromophore, whilst emission occurs from a configuration in which the excitation delocalizes over both chromophores. Such a scenario could readily arise as the cleft angle in **(ZnP)₂** is quite flexible, allowing the porphyrins to either approach each other closely or stay apart depending on the electronic states of the rings.

Similarly, **(2HP)₂** also illustrates a larger Stokes shift than that of **2HP** and a depressed sideband (Fig. S4d). The sideband emission of **ZnP** is depressed compared to the sideband absorption, analogous to the observations for **2HP** described earlier, due to the vibronic origin of the band. However, the emission sidebands for **(ZnP)₂** and **(2HP)₂** are depressed much further. Full delocalization of the excited-state excitation would be expected to halve the sideband intensity, in rough agreement with the observation. Again absorption appears to occur to a localized state whilst emission occurs after geometrically induced delocalization.

The UV-vis absorption spectra of $(\text{ZnP})_2\text{Q-Q2HP-C}_{60}$ and $(\text{2HP})_2\text{Q-Q2HP-C}_{60}$ shown in Fig. S5a illustrate significantly broadened Soret bands compared to the spectra of the components $(\text{ZnP})_2$, $(\text{2HP})_2$ and Q2HP-C_{60} , which indicates the presence of intramolecular interactions through the Qx-Qx linkages. From the co-plot of the absorption and emission spectra of $(\text{ZnP})_2\text{Q-Q2HP-C}_{60}$ (Fig. S5b), an absorption band at ca. 15700 cm^{-1} , is assigned to $(\text{ZnP})_2\text{Q}$. The emission spectrum of $(\text{ZnP})_2\text{Q-Q2HP-C}_{60}$ in Fig. S5b displays **essentially** only 2HPQ fluorescence, indicating $(\text{ZnP})_2\text{Q}$ to 2HPQ intramolecular singlet-singlet energy transfer. Based on the anticipated emission/absorption asymmetry, the absorption sequence structure is also assigned in this figure, revealing clear features associated with 2HPQ but only one clearly identified absorption for $(\text{ZnP})_2\text{Q}$, at 15650 cm^{-1} . However, based on Fig. S2c, the observed peak at 17600 cm^{-1} appears disproportionately strong to arise purely from 2HPQ, and this band is therefore presumed to arise primarily from $(\text{ZnP})_2\text{Q}$. Hence, the absorption spectrum of $(\text{ZnP})_2\text{Q}$ appears to consist of the sums of the absorption spectra of the individual chromophores ZnP and ZnPQ (see Figs. 5a and 6a), quite different from the spectrum of $(\text{ZnP})_2$ (see Fig. S4a). This indicates that any exciton delocalization in $(\text{ZnP})_2$ is lost in $(\text{ZnP})_2\text{Q}$ owing to the reduced symmetry.

For $(\text{2HP})_2\text{Q-Q2HP-C}_{60}$, the lowest-energy porphyrin absorption band arises from the Tröger's base $(\text{2HP})_2\text{Q}$ rather than from 2HPQ (Fig. S5c). Also, the spectrum of the $(\text{2HP})_2\text{Q}$ component appears to match that for $(\text{2HP})_2$, indicating that asymmetry introduced by the fusion of the bridging quinoxalinyll group does not significantly alter the exciton coupling from that in $(\text{2HP})_2$, as perceived from Fig. S4d. Hence, $(\text{2HP})_2\text{Q-Q2HP-C}_{60}$ illustrates quite different fluorescence from that of $(\text{ZnP})_2\text{Q-Q2HP-C}_{60}$, with the observed emission of $(\text{2HP})_2\text{Q-Q2HP-C}_{60}$ (Fig. S5c) coming from $(\text{2HP})_2\text{Q}$ instead of from Q2HP. However, this intensity is again strongly quenched by the presence of the fullerene group. A possible interpretation of this is that intramolecular singlet-singlet energy transfer takes place from the singlet excited state of the fullerene-appended 2HPQ (1.88 eV) to the energetically lower lying $(\text{2HP})_2\text{Q}$ ($1.80 \pm 0.01\text{ eV}$) and that this state then initiates photochemical charge separation. This is an unlikely scenario, however,

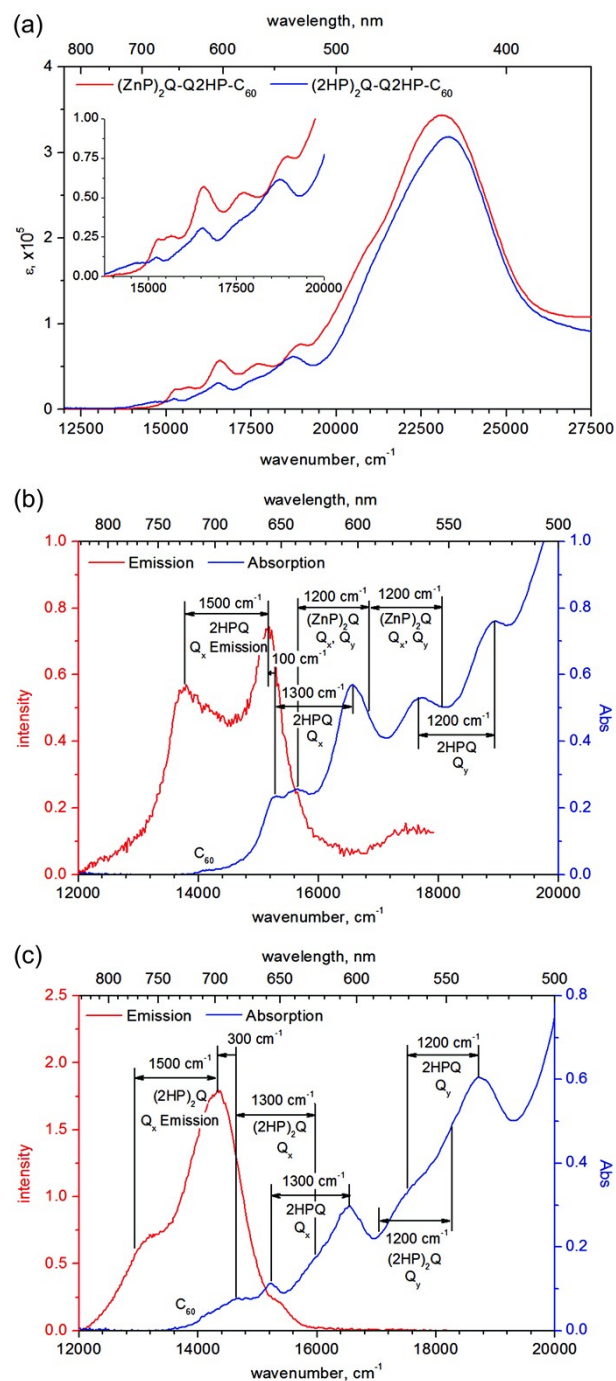


Fig. S5. (a) UV-visible absorption spectra indicating the molar extinction coefficients ϵ (in $\text{M}^{-1}\text{ cm}^{-1}$) of $(\text{ZnP})_2\text{Q-Q2HP-C}_{60}$ and $(\text{2HP})_2\text{Q-Q2HP-C}_{60}$ in PhCN. Co-plot of emission and UV-visible absorption spectra of (b) $(\text{ZnP})_2\text{Q-Q2HP-C}_{60}$; and (c) $(\text{2HP})_2\text{Q-Q2HP-C}_{60}$ in PhCN. For the fluorescence experiment, a wavelength of 550 nm was used for excitation.

as $(2\text{HP})_2\text{Q}$ and C_{60} are far apart in the molecule. An alternative explanation is that $^1(2\text{HPQ})^*$ initiates charge separation and hence disappears quickly whilst $^1(2\text{HP})_2\text{Q}^*$ lives longer as it must be first converted endothermically to $^1(2\text{HPQ})^*$ before quenching.

S3. Electrochemistry

Figure S6 shows the observed cyclic voltammograms for systems Q2HP-C_{60} , ZnPQ-Q2HP-C_{60} , $(\text{ZnP})_2\text{Q-Q2HP-C}_{60}$ and $(2\text{HP})_2\text{Q-Q2HP-C}_{60}$ whose redox data are summarized in Table 2 of the main text.

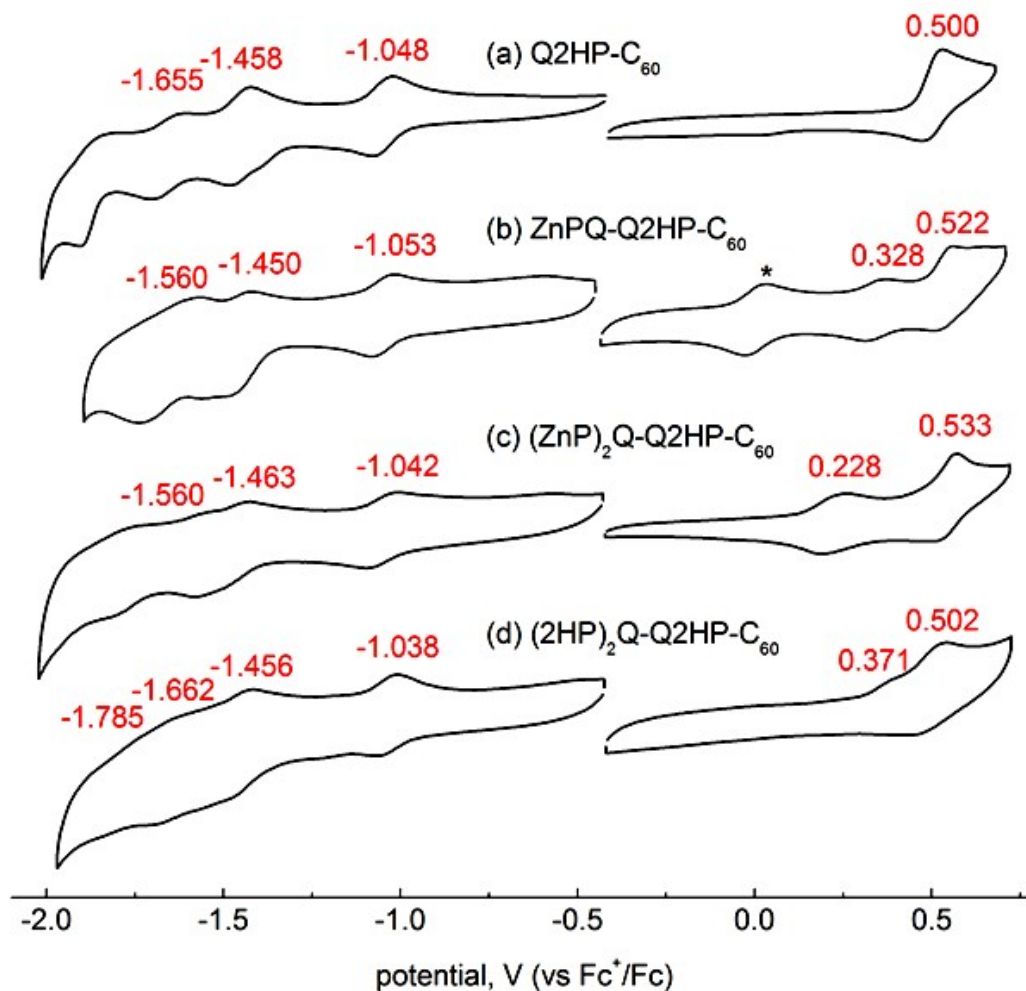


Fig. S6 Cyclic voltammograms of Q2HP-C_{60} , ZnPQ-Q2HP-C_{60} , $(\text{ZnP})_2\text{Q-Q2HP-C}_{60}$ and $(2\text{HP})_2\text{Q-Q2HP-C}_{60}$ in deaerated PhCN containing 0.10 M $n\text{-Bu}_4\text{NPF}_6$ at 298 K. The asterisked signal arises from ferrocene which acts as an internal reference.

Figure S7 shows the observed cyclic voltammograms for model systems **ZnP**, **(ZnP)₂**, **2HP**, **(2HP)₂**, **Q2HP-Ph** and **Ph-C₆₀** whose redox data are summarized in Table 2 of the main text.

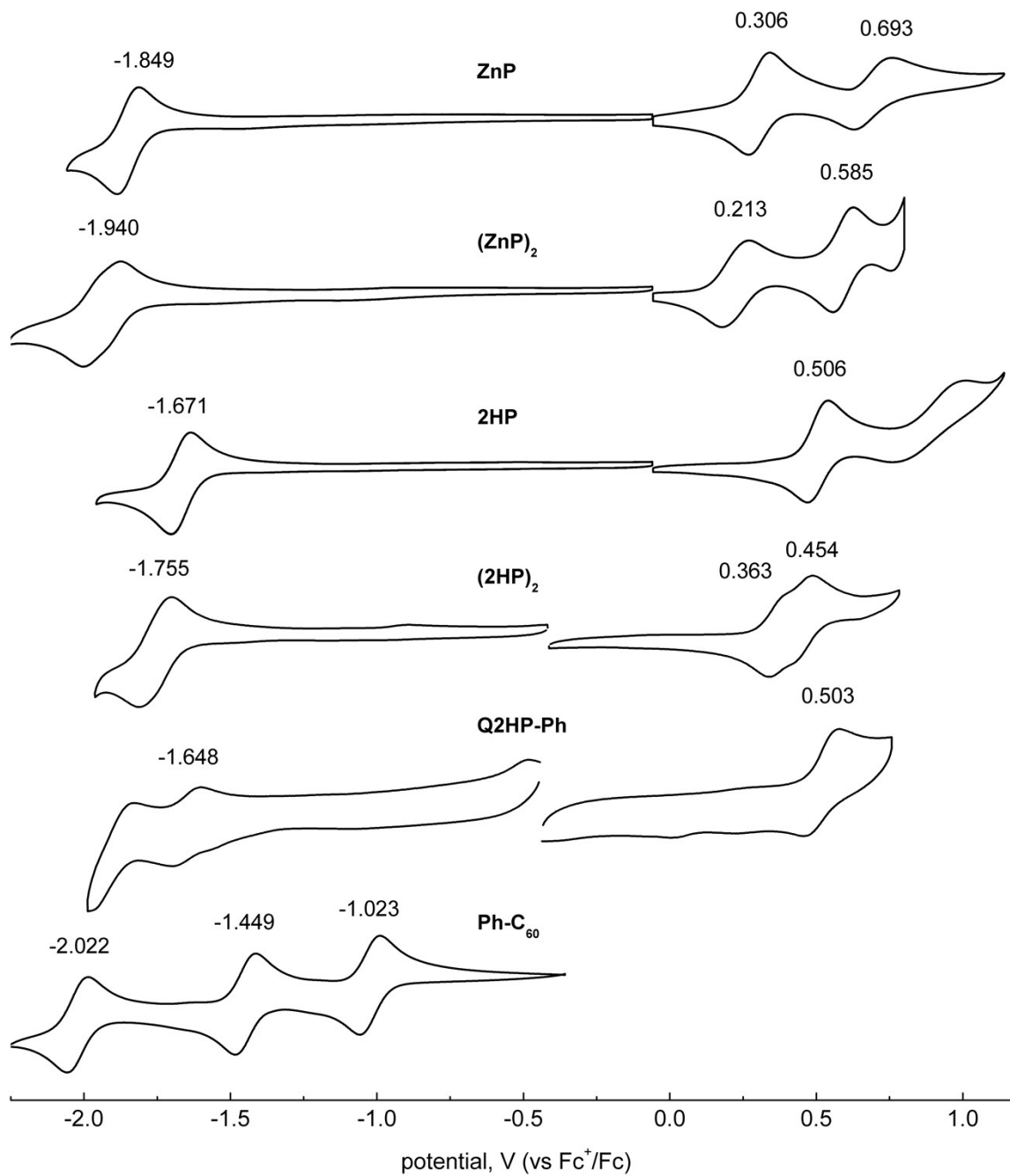
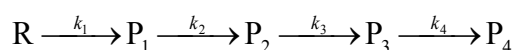


Fig. S7 Cyclic voltammograms of **ZnP**, **(ZnP)₂**, **2HP**, **(2HP)₂**, **Q2HP-Ph** and **Ph-C₆₀** in deaerated PhCN containing 0.10 M *n*-Bu₄NPF₆ at 298 K.

S4. Fitting of Data Measured by Femtosecond Laser Flash Photolysis

Figures S8 – S11 show in their leftmost frames the observed femtosecond time-resolved transient absorption spectra $\Delta A(\nu, t)$ after smoothing and expression on scales linear in frequency and logarithmic in time. These images are the same as those shown in the main text as Figs. 2a, 3a, 4a and 5a but scales are added showing the absorbance values associated with each color. Shown in the centre frame of Figure S8 is the fit to this data obtained based on kinetics schemes of the form



where R is the unexcited ground-state of the system and the identity of the other product components P_i vary, as depicted in Fig 2e. For the other molecules, the kinetics scheme used involves branching and multiple pathways, as described in Fig. 3e, Fig 4e, and Fig 5e.

This procedure extracts the rate constants k and hence the associated isolated-component rise times $\tau = 1/k$, as well as the spectra of each of the product components. The deduced spectral components $\Delta A_i(\nu)$ are shown in Figs. 2, 3, 4 and 5, while the rise times are given in Table 3. The right-most frames in Figs. S3 – S6 show the relative concentration of each component as a function of time.

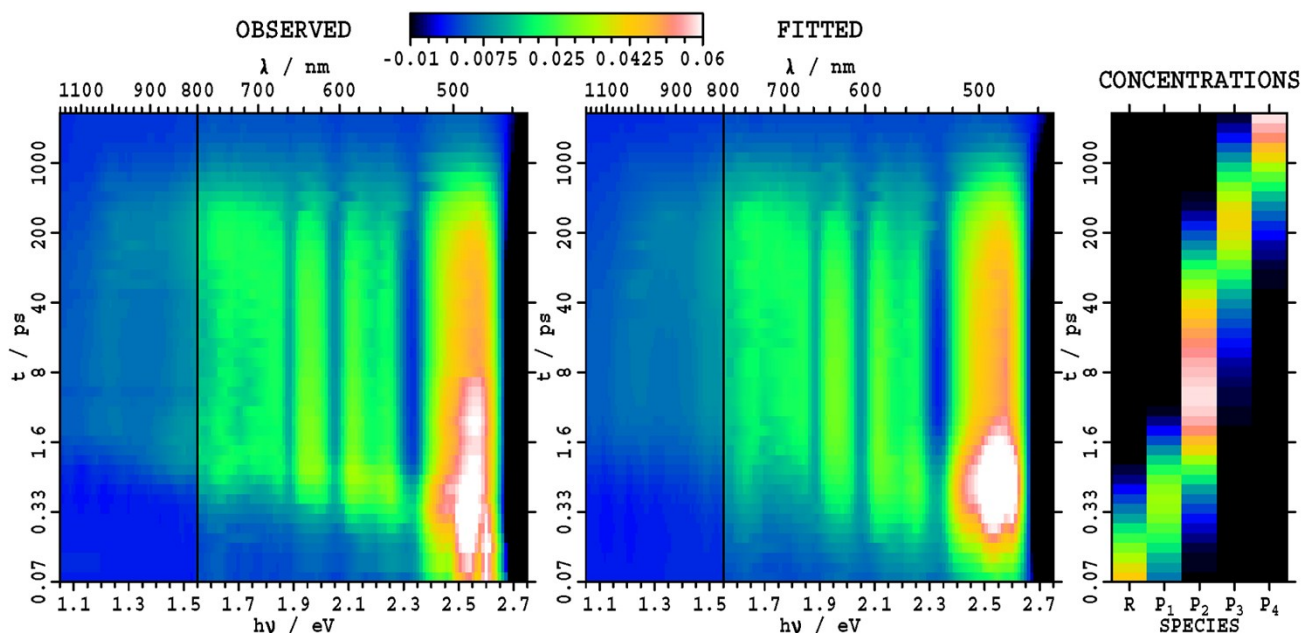


Fig. S8 Observed and fitted transient absorption spectra $\Delta A(\nu, t)$ following excitation at 430 nm in PhCN at 298 K of Q2HP-C₆₀ and the time profiles of the relative concentrations (black = 0%, white = 100%) of the fitted components R – P₄.

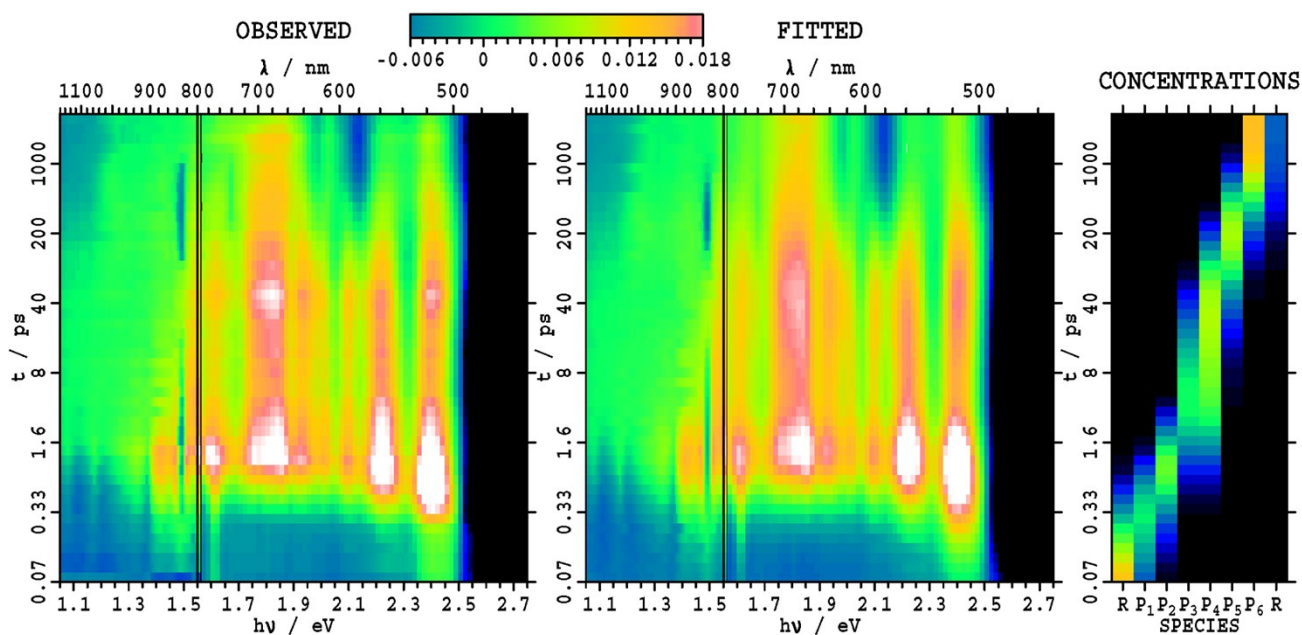


Fig. S9 Observed and fitted transient absorption spectra $\Delta A(v,t)$ following excitation at 430 nm in PhCN at 298 K of ZnPQ-Q2HP-C₆₀ and the time profiles of the relative concentrations (black = 0%, white = 100%) of the fitted components R – P₆.

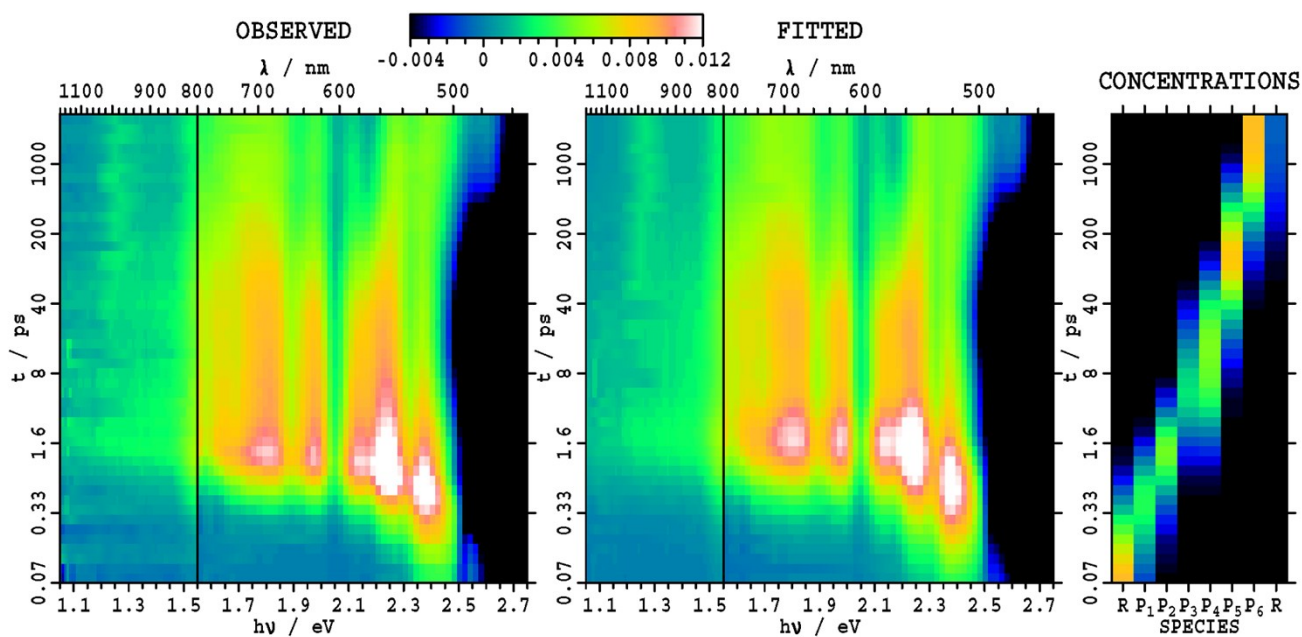


Fig. S10 Observed and fitted transient absorption spectra $\Delta A(v,t)$ following excitation at 298 K of (ZnP)₂Q-Q2HP-C₆₀ and the time profiles of the relative concentrations (black = 0%, white = 100%) of the fitted components R – P₅.

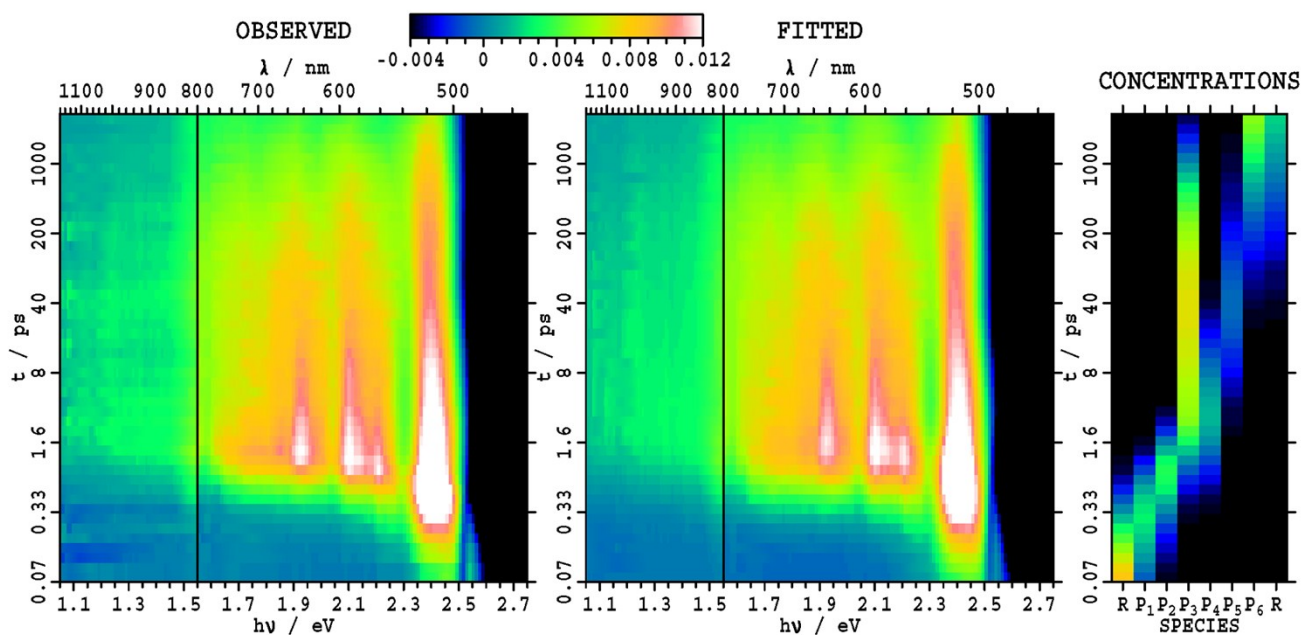


Fig. S11 Observed and fitted transient absorption spectra $\Delta A(\nu, t)$ following excitation at 430 nm in PhCN at 298 K of $(2\text{HP})_2\text{Q-Q2HP-C}_{60}$ and the time profiles of the relative concentrations (black = 0%, white = 100%) of the fitted components R – P₄.

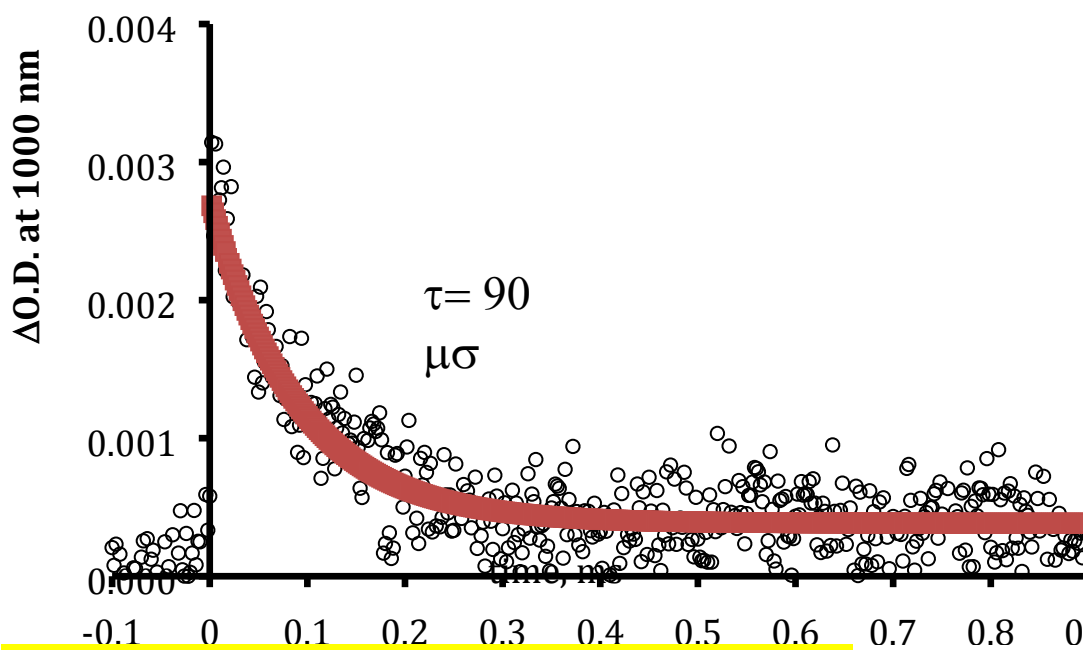


Fig. S12 The time decay profile for $(2\text{HP})_2\text{Q-Q2HP-C}_{60}$ of the optical density at 1000 nm.

S5. Spectroelectrochemistry of (2HP)₂

Figure S13 shows the observed UV-visible absorption spectral changes and the differential spectra for the oxidations of (2HP)₂ in PhCN.

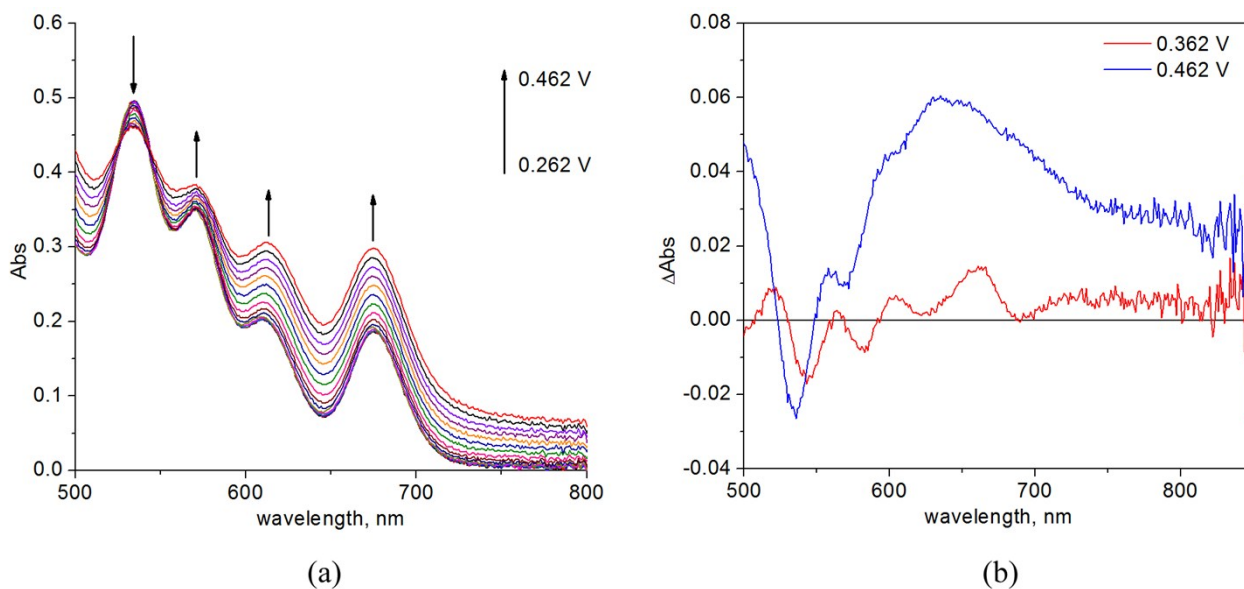


Fig. S13 (a) UV-visible absorption spectral changes for the oxidations of (2HP)₂ in PhCN; (b) differential absorption spectra for the oxidation of (2HP)₂ in PhCN. The spectrum with the applied potential of 0.362 V (vs Fc⁺/Fc) (red) refers to the first oxidation of a single porphyrin to give [2HP-2HP]^{•+}, while the spectrum with the applied potential 0.462 V refers to the oxidation of both porphyrins to give 2HP^{•+}-2HP^{•+}.

S6. Vibrational Parameters Deduced for the Molecular Fragments from B3LYP Vibrational Frequency Analysis

B3LYP calculations are performed for the neutral and ionized forms of the porphyrin and fullerene fragments. These fragments include the neighbouring joining groups such as imidazole and phenyl rings. The total intramolecular reorganization energy λ_i is determined from the difference in total electronic energy between the vertically excited and equilibrium structures of the ions. These are then partitioned into contributions from the normal modes by curvilinear projection. Only the modes with large displacement are included in the calculations, with the displacement of these modes renormalized so as to preserve the total intramolecular reorganization energy. The included mode frequencies and dimensionless displacements are given in Table S1.

Table S1 Vibrational parameters used in the determination of Franck-Condon factors for charge-transfer processes^a

Mode	P-P ⁺ ($\lambda_i = 0.036$ eV)		C ₆₀ -C ₆₀ ⁻ ($\lambda_i = 0.116$ eV)	
	Freq.	Displ.	Freq.	Displ.
1	44	1.401	149	1.280
2	76	1.683	650	0.546
3	1454	0.230	1233	0.460
4	1556	0.297	1408	0.680
5	-	-	1477	0.415
6	-	-	1524	0.393

^a The vibration frequencies are in cm⁻¹ while dimensionless displacements are given. The Huang-Rhys factor S is given by (displacement)²/2.

S7. References

1. M. J. Crossley, C. S. Sheehan, T. Khoury, J. R. Reimers and P. J. Sentic, *New J. Chem.*, 2008, **32**, 340.
2. Z. Ou, W. E, J. Shao, P. L. Burn, C. S. Sheehan, R. Walton, K. M. Kadish and M. J. Crossley, *J. Porphyrins Phthalocyanines*, 2005, **9**, 142.
3. K. M. Kadish, W. E, P. J. Sentic, Z. Ou, J. Shao, K. Ohkubo, S. Fukuzumi, L. J. Govenlock, J. A. McDonald, A. C. Try, Z.-L. Cai, J. R. Reimers and M. J. Crossley, *J. Phys. Chem. B*, 2007, **111**, 8762.
4. P. J. Sentic, W. E, Z. Ou, J. Shao, J. A. McDonald, Z.-L. Cai, K. M. Kadish, M. J. Crossley and J. R. Reimers, *Phys. Chem. Chem. Phys.*, 2008, **10**, 268. This article was unfortunately duplicated later in 10(4) P515-527, their note 10 P7328.
5. K. Sendt, L. A. Johnston, W. A. Hough, M. J. Crossley, N. S. Hush and J. R. Reimers, *J. Am. Chem. Soc.*, 2002, **124**, 9299.
6. P. Atkins and J. de Paula, *Atkins' Physical Chemistry*, 9 edn., Oxford University press, Oxford, 2010.
7. M. Gouterman, *J. Molec. Spectrosc.*, 1961, **6**, 138.
8. R. L. Fulton and M. Gouterman, *J. Chem. Phys.*, 1961, **35**, 1059.
9. R. L. Fulton and M. Gouterman, *J. Chem. Phys.*, 1964, **41**, 2280.
10. M. Gouterman, *The Journal of Chemical Physics*, 1965, **42**, 351.
11. G. Fischer, *Vibronic Coupling*, Academic Press, London, 1984.
12. E. K. L. Yeow, P. J. Sentic, N. M. Cabral, J. N. H. Reek, M. J. Crossley and K. P. Ghiggino, *Phys. Chem. Chem. Phys.*, 2000, **2**, 4281.
13. M. J. Crossley, P. J. Sentic, J. A. Hutchison and K. P. Ghiggino, *Org. Biomol. Chem.*, 2005, **3**, 852.
14. H. Imahori, K. Tamaki, D. M. Guldi, C. Luo, M. Fujitsuka, O. Ito, Y. Sakata and S. Fukuzumi, *J. Am. Chem. Soc.*, 2001, **123**, 2607.
15. K. Tamaki, H. Imahori, Y. Sakata, Y. Nishimura and I. Yamazaki, *Chem. Commun. (Cambridge, U. K.)*, 1999, 625.
16. C. Luo, D. M. Guldi, H. Imahori, K. Tamaki and Y. Sakata, *J. Am. Chem. Soc.*, 2000, **122**, 6535.
17. S. I. Yang, R. K. Lammi, J. Seth, J. A. Riggs, T. Arai, D. Kim, D. F. Bocian, D. Holten and J. S. Lindsey, *J. Phys. Chem. B*, 1998, **102**, 9426.
18. K. Kilsa, J. Kajanus, J. Martensson and B. Albinsson, *J. Phys. Chem. B*, 1999, **103**, 7329.